Double-Quadrant State-of-Charge-Based Droop Control Method for Distributed Energy Storage Systems in Autonomous DC Microgrids

Xiaonan Lu, *Member*, *IEEE*, Kai Sun, *Member*, *IEEE*, Josep M. Guerrero, *Senior Member*, *IEEE*, Juan C. Vasquez, *Member*, *IEEE*, and Lipei Huang

***Abstract*—In this paper, a double-quadrant state-of-charge (SoC)-based droop control method for distributed energy storage system is proposed to reach the proper power distribution in autonomous dc microgrids. In order to prolong the lifetime of the energy storage units (ESUs) and avoid the overuse of a certain unit, the SoC of each unit should be balanced and the injected/output power should be gradually equalized. Droop control as a decentralized approach is used as the basis of the power sharing method for distributed energy storage units. In the charging process, the droop coefficient is set to be proportional to the *n*th order of SoC, while in the discharging process, the droop coefficient is set to be inversely proportional to the *n*th order of SoC. Since the injected/output power is inversely proportional to the droop coefficient, it is obtained that in the charging process the ESU with higher SoC absorbs less power, while the one with lower SoC absorbs more power. Meanwhile, in the discharging process, the ESU with higher SoC delivers more power and the one with lower SoC delivers less power. Hence, SoC balancing and injected/output power equalization can be gradually realized. The exponent *n* of SoC is employed in the control diagram to regulate the speed of SoC balancing. It is found that with larger exponent *n*, the balancing speed is higher. MATLAB/simulink model comprised of three ESUs is implemented and the simulation results are shown to verify the proposed approach.**

***Index Terms*—DC microgrid, distributed energy storage unit (DESU), droop control, state-of-charge (SoC).**

I. Introduction

WITH THE development of modern electric power system, renewable energy and microgrid have gained more awareness nowadays [1]–[3]. Since the conventional electric grid is implemented based on ac system, ac microgrids have drawn more attention [4]–[8]. However, various sources and loads in a microgrid have dc couplings, e.g., photovoltaics (PVs), batteries, LEDs, etc. Hence, it is simpler and more efficient to connect them with dc–dc converters to form a dc microgrid. In contrast to ac microgrids, dc microgrids do not have the problems caused by harmonics and reactive power, and can operate with higher efficiency. Considering the above advantages, dc microgrid has been intensively studied recently [9]–[16]. The configuration of a typical dc microgrid is shown in Fig. 1 [13].

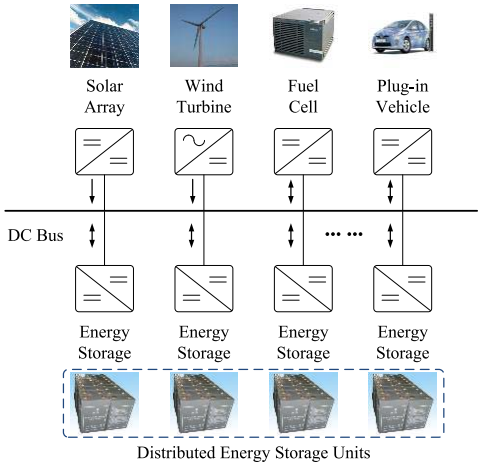

Fig. 1. Typical configuration of a dc microgrid.

In order to connect the renewable energy sources and the loads, power electronics converters are usually employed as the interfaces [17]. Power sharing between different interfacing converters is a key problem in the control system design of microgrids [4]–[8], [11], [14]–[16]. Different approaches have been proposed in [4]–[8], [11], [13]–[16], [18]–[20], among them droop control and its variants as decentralized methods have been widely studied [4]–[8], [11], [13]–[16]. In a dc microgrid, droop control is achieved by reducing the dc voltage reference value as the load power increases. Hence, the output power of each interfacing converter can be automatically equalized by regulating the dc output voltage.

Although renewable energy sources have many advantages, their output power possesses the stochastic and intermittent properties. In order to solve these problems, the energy storage units (ESUs) should be employed to restrain the power

Manuscript received February 18, 2014; revised June 29, 2014; accepted August 12, 2014. Date of publication September 11, 2014; date of current version December 17, 2014. This work was supported by the National Natural Science Foundation of China under Grant 51177083. Paper no. TSG-00125-2014.

X. Lu is with the Department of Electrical Engineering and Computer Science, University of Tennessee, Knoxville TN 37996 USA.

K. Sun and L. Huang are with the State Key Laboratory of Power Systems, Department of Electrical Engineering, Tsinghua University, Beijing 100084, China (e-mail: sun-kai@mail.tsinghua.edu.cn).

J. M. Guerrero is with the Institute of Energy Technology, Aalborg University, Aalborg 9220, Denmark; and also with the Control Science and Engineering College, Shandong University, Jinan 250061, China.

J. C. Vasquez is with the Institute of Energy Technology, Aalborg University, Aalborg 9220, Denmark.

Color versions of one or more of the figures in this paper are available online at http://ieeexplore.ieee.org.

Digital Object Identifier 10.1109/TSG.2014.2352342

fluctuation [21]. Considering the distributed connection of the sources and loads in a microgrid, distributed ESUs (DESUs) are commonly used [11], [14]. An ESU is usually comprised of series-connected battery cells, and the whole ESU consisting of the above battery cells is connected to the common bus with power electronics interfacing converter. The control system of the ESUs is composed of two parts. They are battery management system (BMS) and power converter system (PCS), respectively [14]. The function of BMS is to monitor the status of each battery unit in an ESU and to balance the state-of-charge (SoC) of each cell. Meanwhile, the function of PCS is to control the output voltage and current, and also to reach the proper load power sharing.

In order to efficiently use the DESUs and prolong their service life, two requirements regarding SoC should be satisfied. First, the SoC of each cell in the battery string of an ESU should be balanced. Second, the SoC of the whole ESU should be balanced among different ESUs. The first requirement can be achieved by using the BMS, and the second can be achieved by using the PCS. Literatures have shown some work on the above requirements. For BMS, in [22] the intramodule equalizers are employed to balance the SoCs of different units in a battery string. In [23], the redundant cell is used, with which the balanced SoC can be obtained by dynamically disconnecting the cell whose SoC does not match the others'. In [24], the screening process is employed to improve the performance of SoC balancing in a string of battery cells. For PCS, in [25], a cascade H-bridge topology is employed and the SoC of each ESU is controlled directly to make them equal with each other among different ESUs. In [11], a gain-scheduling droop control method is modified by using fuzzy control, in order that the SoC and output power of each ESU is gradually balanced. In [14], the droop coefficient is calculated by using the SoC in the discharging process, so the output power of each unit is in proportion to the corresponding SoC.

This paper focuses on the control system of PCS. As aforementioned, the ESUs are dispersedly connected to the common bus in a microgrid. Hence, decentralized control scheme for the PCS is preferred. However, in [25], different ESUs are connected to the isolated dc terminals in the cascade H-bridges, and centralized control method is used to reach the SoC balancing. As a result, this method is suitable for the centralized application, such as battery chargers for hybrid electric vehicles, while it does not meet the requirement of microgrids. In [11], although the proposed method is realized based on the decentralized droop control method, the communication between different ESUs are needed to calculate the average energy. The approach proposed in [14] is achieved only based on the local information, e.g., SoC, output voltage, etc. However, different operation modes are not fully considered. Only the discharge process of the ESU is taken into account. In order to reach the SoC balancing in different operation modes, the feasibility of the proposed method should be further extended.

In this paper, aiming at PCS, the decentralized control system based on droop control is developed to balance the SoC of each ESU and equalize their injected/output power in an autonomous dc microgrid. In particular, in the charging operation mode, the droop coefficient is set to be proportional to the nth order of SoC, while in the discharging operation mode, the droop coefficient is set to be inversely proportional to the nth order of SoC. Hence, in both of the above operation modes, the SoC of each ESU can be gradually balanced, and the injected/output power is thereby equalized. It should be noticed that the exponent n is employed in the above method to regulate the power sharing speed. It can be demonstrated that with larger exponent n, the SoC balancing and power sharing speed can be enhanced.

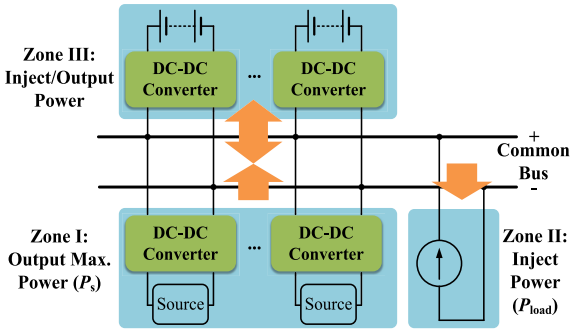

Fig. 2. Configuration of an autonomous dc microgrid.

The following paper is summarized as follows. Section II shows the operation principle of the autonomous dc microgrids. Section III analyzes the double-quadrant SoC-based droop control method in detail. The principle of the proposed approach is explained and the stability analysis is performed. Meanwhile, the speed regulation of SoC balancing and power sharing is studied. The limitations of the parameters in the control scheme are also discussed. Section IV shows the simulation tests, which are used to validate the proposed control method. Finally, Section V summarizes the paper and draws the conclusion.

II. Operation Principle of Autonomous DC Microgrids With DESUs

The configuration of an autonomous dc microgrid is shown in Fig. 2, which is comprised of three zones: I—sources, II—loads, and III—DESUs. Zone I is formed by the distributed renewable energy sources, which operate in maximum power point tracking (MPPT) mode and output power into the common bus. Zone II is formed by the loads, in which the power is injected from the common bus. As mentioned above in Section I, considering the stochastic and intermittent property of the sources in Zone I and also the load variation in Zone II, DESUs should be employed in the dc microgrids, as shown in Zone III. When the power generated (P_s) in Zone I is higher than the power consumed (P_{load}) in Zone II, sufficient power is supplied in the system and the DESUs operate in the charging mode. On the other hand, when the power generated in Zone I is lower than the power consumed in Zone II, the power in the system is not enough to feed the loads. Hence, the DESUs operate in the discharging mode to match the power difference.

During the operation of DESUs, it is necessary to balance the SoC of each ESU and equalize the power. Hence, the overuse of a certain unit can be avoided and the lifetime of

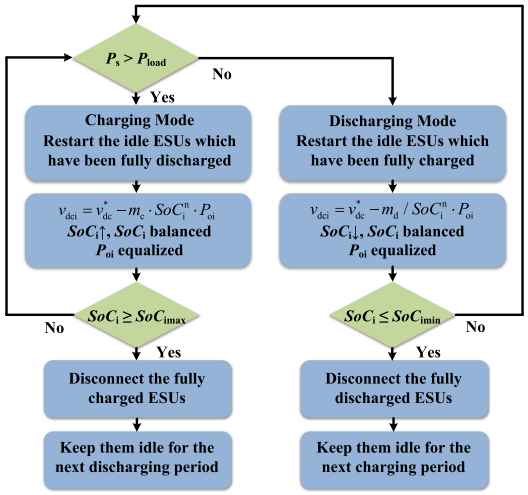

Fig. 3. Flow chart of the operation principle for autonomous dc microgrids.

the energy storage system is prolonged. In particular, in the charging process, the fully discharged ESU is restarted and the droop coefficient in the control system for each ESU is set to be proportional to SoC^n. When the ESU reaches its maximum acceptable SoC during charging, it is disconnected to wait for the next discharging process. Meanwhile, in the discharging process, the fully charged ESU is restarted and the droop coefficient is set to be inversely proportional to the SoC^n. When the ESU reaches its minimum SoC, it is disconnected to wait for the next charging process. The flow chart of the above operation principle for autonomous dc microgrids is shown in Fig. 3.

III. Double-Quadrant SoC-Based Droop Control Method

A. Principle of Proposed Method

As aforementioned, the SoC balancing and injected/output power equalization should be achieved in both charging and discharging modes. The conventional droop curve in the first quadrant can be extended to obtain the double-quadrant droop curve. The part of the droop curve in the first quadrant represents the discharging process, and the part in the second quadrant represents the charging process. The overall diagram for the double-quadrant SoC-based droop control method is shown in Fig. 4. It is seen that in the charging mode, with higher SoC the injected power (absolute value) is lower, and with lower SoC the injected power (absolute value) is higher. In the discharging mode, with higher SoC the output power is higher, and with lower SoC the output power is lower.

The expression of droop control in dc microgrids can be shown as

$$v_{\mathrm{dci}}^* = v_{\mathrm{dc}}^* - m_{\mathrm{i}} \cdot P_{\mathrm{oi}} \tag{1}$$

where $v_{\mathrm{dci}}{}^*$, m_{i}, and P_{oi} are the reference of dc output voltage, droop coefficient and filtered power by the low-pass filter (LPF) of converter #*i* respectively ($i = 1, 2, \ldots, k$), $v_{\mathrm{dc}}{}^*$ is the reference of dc output voltage at no-load condition.

It should be noticed that P_{oi} is positive in the discharging process and negative in the charging process.

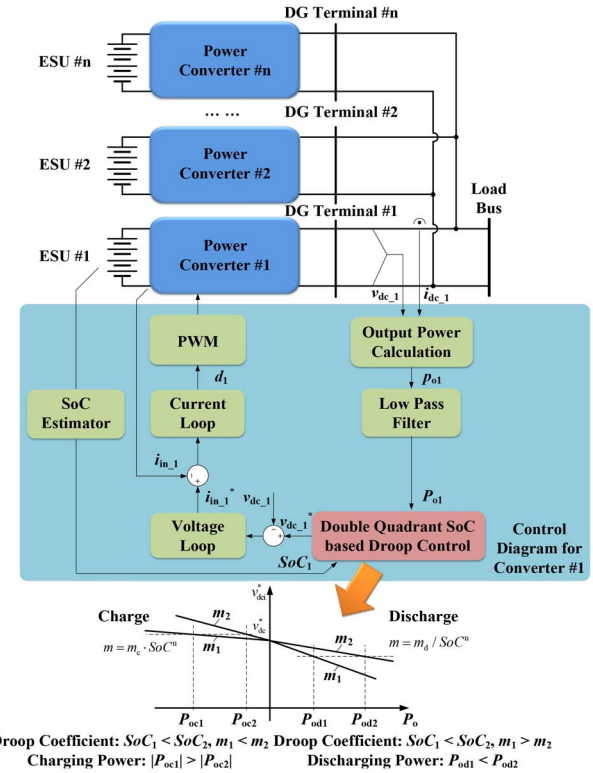

Fig. 4. Overall control diagram including the double-quadrant SoC-based droop control method.

In order to meet the requirement of SoC balancing, in the charging operation mode, the droop coefficient is set to be

$$m_{\mathrm{i}} = m_{\mathrm{c}} \cdot \mathrm{SoC}_{\mathrm{i}}^n \tag{2}$$

where m_{c} is the droop coefficient for charging process when $\mathrm{SoC_i}$ equals 100%, n is the exponent of SoC, which is involved to regulate the speed of SoC balancing.

The sizing of a dc cable can be found in [26] and [27]. It is shown that the line resistance of the dc cable should be designed to make the voltage drop across the cable less than 5% of the rated voltage regardless of the cable length. Fig. 5 shows the line resistance per unit length and the corresponding sectional area for different cable length at 20 °C and 90 °C. It is shown that with longer cable, the line resistance per unit length should be reduced accordingly.

Since the line resistance is designed to guarantee the acceptable voltage drop, it yields

$$v_{\mathrm{dc1}} \approx \cdots \approx v_{\mathrm{dck}} \approx v_{\mathrm{dcload}}. \tag{3}$$

Considering that the ideal voltage controller is used, the actual dc output voltage is equal to its reference value. Combining (1)–(3), it is derived

$$P_{\mathrm{o1}} : P_{\mathrm{o2}} : \cdots : P_{\mathrm{ok}} = \frac{1}{\mathrm{SoC}_1^n} : \frac{1}{\mathrm{SoC}_2^n} : \cdots : \frac{1}{\mathrm{SoC}_{\mathrm{k}}^n}. \tag{4}$$

It is concluded from (4) that in the charging operation mode, if $\mathrm{SoC_i} > \mathrm{SoC_j}$ ($i, j = 1, 2, \ldots, k$), then $|P_{\mathrm{oi}}| < |P_{\mathrm{oj}}|$. It means that the increasing speed of $\mathrm{SoC_i}$ is lower than $\mathrm{SoC_j}$. Hence, $\mathrm{SoC_i}$ and $\mathrm{SoC_j}$ are gradually balanced. Meanwhile, the injected power is thereby equalized.

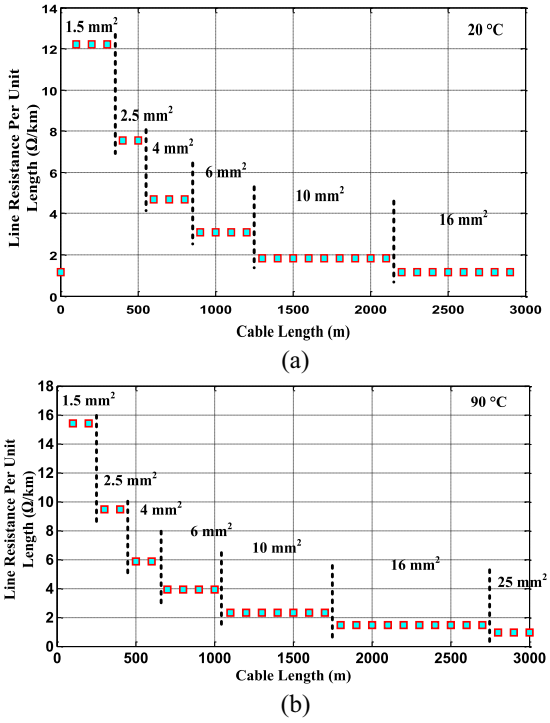

Fig. 5. Line resistance per unit length and the corresponding sectional area. (a) 20 °C. (b) 90 °C.

Meanwhile, in the discharging operation mode, the droop coefficient is set to be

$$m_{\mathrm{i}} = \frac{m_{\mathrm{d}}}{\mathrm{SoC}_{\mathrm{i}}^{n}} \tag{5}$$

where m_{d} is the droop coefficient for discharging process when $\mathrm{SoC_i}$ equals 100%, n is the exponent of SoC which is involved to regulate the speed of SoC balancing.

As same as the condition in the charging process, the voltage drop across the power line can be neglected. Therefore, (3) is also satisfied. Combining (1), (3), and (5), it is reached

$$P_{\mathrm{o1}} : P_{\mathrm{o2}} : \cdots : P_{\mathrm{ok}} = \mathrm{SoC}_1^n : \mathrm{SoC}_2^n : \cdots : \mathrm{SoC}_{\mathrm{k}}^n. \tag{6}$$

It is concluded from (6) that in the discharging operation mode, if $\mathrm{SoC_i} > \mathrm{SoC_j}$ ($i, j = 1, 2, \ldots, k$), then $P_{\mathrm{oi}} > P_{\mathrm{oj}}$. It means that the decreasing speed of $\mathrm{SoC_i}$ is higher than $\mathrm{SoC_j}$. Hence, $\mathrm{SoC_i}$ and $\mathrm{SoC_j}$ are gradually balanced. Meanwhile, the output power of ESU #i and ESU #j is equalized.

Here, the coulomb counting method is used to obtain the SoC of each ESU, which is shown as

$$\mathrm{SoC_i} = \mathrm{SoC_{it=0}} - \frac{1}{C_{\mathrm{ei}}} \int i_{\mathrm{oei}} \mathrm{d}t \tag{7}$$

where $\mathrm{SoC_{it=0}}$ is the initial $\mathrm{SoC_i}$ at the starting time, C_{ei} and i_{oei} are the capacity and output current of the ESU #i.

Meanwhile, considering the power balancing in the input side and output side of the interfacing converter, it yields

$$p_{\mathrm{oi}} \approx p_{\mathrm{oei}} = v_{\mathrm{oei}} i_{\mathrm{oei}} \tag{8}$$

where p_{oi} is the injected/output power of converter #i before low-pass filtering, v_{oei} is the output voltage of ESU #i, p_{oei} and i_{oei} are the injected/output power and current, respectively.

TABLE I
SYSTEM PARAMETERS

Item	Symbol	Value	Unit
Initial SoC of ESU #1	$SoC_{1\,t=0}$	0.6/0.9	1
Initial SoC of ESU #2	$SoC_{2\,t=0}$	0.5/0.8	1
Initial SoC of ESU #3	$SoC_{3\,t=0}$	0.4/0.7	1
Converter Output Voltage	V_{o}	600	V
Converter Input Voltage	V_{in}	200	V
Difference between Source Power and Load Power	P_{req}	-3/3	kW
Max. Power Rating of Each Converter	p_{max}	2.5	kW
Max. DC Voltage Deviation	$\Delta v_{\mathrm{dcmax}}$	$5\% \cdot V_{\mathrm{rated}}$	V
Min. DC Voltage Deviation	$\Delta v_{\mathrm{dcmin}}$	$3.3‰ \cdot V_{\mathrm{rated}}$	mV

Since the output voltage of the ESU almost keeps constant in a large range of SoC, it is assumed that v_{oei} is a constant value in (8). Hence, combining (7) and (8), it is derived

$$\mathrm{SoC_i} = \mathrm{SoC_{it=0}} - \frac{1}{C_{\mathrm{ei}} v_{\mathrm{oei}}} \int p_{\mathrm{oi}} \mathrm{d}t. \tag{9}$$

At the same time, considering the power matching in the system, it is reached

$$P_{\mathrm{req}} = -\left(P_{\mathrm{s}} - p_{\mathrm{load}}\right) = \sum_{\mathrm{r}=1}^{k} P_{\mathrm{or}} \tag{10}$$

where P_{req} is the required power in the system which equals the difference of the total power supplied by the sources (P_{s}) and the total power needed by the loads (p_{load}), the negative sign is defined so that the power is positive during discharging and negative during charging.

Combining (9) and (10) and the proportion shown in (4) and (6), it yields that in the charging operation mode

$$\mathrm{SoC_i} = \mathrm{SoC_{it=0}} - \frac{P_{\mathrm{req}}}{C_{\mathrm{ei}} v_{\mathrm{oei}}} \int \frac{\frac{1}{\mathrm{SoC_i^n}}}{\sum_{\mathrm{r}=1}^{k} \frac{1}{\mathrm{SoC_r^n}}} \mathrm{d}t. \tag{11}$$

In the discharging operation mode

$$\mathrm{SoC_i} = \mathrm{SoC_{it=0}} - \frac{P_{\mathrm{req}}}{C_{\mathrm{ei}} v_{\mathrm{oei}}} \int \frac{\mathrm{SoC_i^n}}{\sum_{\mathrm{r}=1}^{k} \mathrm{SoC_r^n}} \mathrm{d}t. \tag{12}$$

Taking the distributed energy storage system (DESS) with three ESUs as an example, the system parameters are shown in Table I. Here, the exponent n is selected as 6 as an example. By solving (10) and (11), the numeric solutions of SoC in the charging operation mode can be obtained, as shown in Fig. 6(a). Meanwhile, by solving (10) and (12), the numeric solutions of SoC in the discharging operation modes can be obtained, as shown in Fig. 6(b). It is seen in Fig. 6(a) and (b) that the SoC of each ESU gradually becomes equal, which indicates the balanced SoC and equalization of injected/output power.

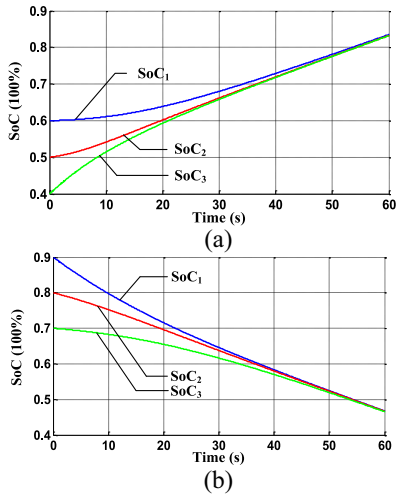

Fig. 6. Numeric solutions of SoC (n = 6). (a) Charging process. (b) Discharging process.

B. Stability Analysis of Proposed Method

The stability of the proposed method can be evaluated by using small signal analysis. In the charging mode, combining (1) and (2) and perturbing the result, it yields

$$\hat{v}_{\rm dci} = -m_{\rm c}{\rm SoC}_{\rm i}^{n}\cdot\hat{P}_{\rm oi} - m_{\rm c}n{\rm SoC}_{\rm i}^{n-1}P_{\rm oi}\cdot\hat{\rm SoC}_{\rm i}. \quad (13)$$

Considering the LPF for the power, it is reached

$$P_{\rm oi} = G_{\rm lpf}\cdot p_{\rm oi}. \quad (14)$$

Here, the first-order LPF is used, which is

$$G_{\rm lpf} = \frac{\omega_{\rm c}}{s+\omega_{\rm c}} \quad (15)$$

where $\omega_{\rm c}$ is the cutting frequency of the LPF.

Perturbing (9) and (14), it is derived

$$\hat{\rm SoC}_{\rm i} = -\frac{\hat{P}_{\rm i}}{sC_{\rm e}V_{\rm oei}G_{\rm lpf}}. \quad (16)$$

Combining (13) and (16), it is obtained that

$$\hat{P}_{\rm oi} = \frac{\lambda_{\rm i}}{m_{\rm c}{\rm SoC}_{\rm i}^{n-1}\left(nP_{\rm oi}-\lambda_{\rm c}{\rm SoC}_{\rm i}\right)}\cdot\hat{v}_{\rm dci} \quad (17)$$

where

$$\lambda_{\rm i} = sC_{\rm e}G_{\rm lpf}V_{\rm oei}. \quad (18)$$

Meanwhile, for the load side, it can be calculated that

$$p_{\rm load} = \frac{v_{\rm dcload}^2}{R_{\rm load}}. \quad (19)$$

Hence, the small signal expression is derived as

$$\hat{p}_{\rm load} = \frac{2V_{\rm dcload}\,\hat{v}_{\rm dcload}}{R_{\rm load}}. \quad (20)$$

Considering the power matching in the system and the expressions in (3), (17), and (20), it is reached that

$$\sum_{\rm r=1}^{k}\frac{\lambda_{\rm r}}{m_{\rm c}{\rm SoC}_{\rm r}^{n-1}\left(nP_{\rm or}-\lambda_{\rm r}{\rm SoC}_{\rm r}\right)} = \frac{2V_{\rm dcload}G_{\rm lpf}}{R_{\rm load}}. \quad (21)$$

Hence, for the sake of simplicity, by taking the system with two ESUs as an example, the characteristic equation can be derived as

$$A_{\rm c}\cdot s^3 + B_{\rm c}\cdot s^2 + C_{\rm c}\cdot s + D_{\rm c} = 0 \quad (22)$$

where

$$\begin{aligned}
A_{\rm c} =& -C_{\rm e}^2R_{\rm load}{\rm SoC}_1{\rm SoC}_2V_{\rm oe1}V_{\rm oe2}\omega^2\left({\rm SoC}_1^n+{\rm SoC}_2^n\right)\\
&+ C_{\rm e}R_{\rm load}{\rm SoC}_1{\rm SoC}_2n\omega\left(P_{\rm o1}{\rm SoC}_1^{n-1}V_{\rm oe2}\right.\\
&\left.+ P_{\rm o2}{\rm SoC}_2^{n-1}V_{\rm oe1}\right)\\
B_{\rm c} =& -2P_{\rm o1}P_{\rm o2}{\rm SoC}_1^n{\rm SoC}_2^nV_{\rm dcload}m_{\rm c}n^2\omega\\
&+ 2C_{\rm e}R_{\rm load}{\rm SoC}_1{\rm SoC}_2n\omega^2\left(P_{\rm o1}V_{\rm oe2}{\rm SoC}_1^{n-1}\right.\\
&\left.+ P_{\rm o2}V_{\rm oe1}{\rm SoC}_2^{n-1}\right)\\
&- C_{\rm e}^2R_{\rm load}{\rm SoC}_1{\rm SoC}_2V_{\rm oe1}V_{\rm oe2}\omega^3\left({\rm SoC}_1^n+{\rm SoC}_2^n\right)\\
&- 2C_{\rm e}^2{\rm SoC}_1^{n+1}{\rm SoC}_2^{n+1}V_{\rm dcload}V_{\rm oe1}V_{\rm oe2}m_{\rm c}\omega^3\\
&+ 2C_{\rm e}{\rm SoC}_1^n{\rm SoC}_2^nV_{\rm dcload}nm_{\rm c}\omega^3\left(P_{\rm o1}{\rm SoC}_2V_{\rm oe2}\right.\\
&\left.+ P_{\rm o2}{\rm SoC}_1V_{\rm oe1}\right)\\
C_{\rm c} =& 4P_{\rm o1}P_{\rm o2}{\rm SoC}_1^n{\rm SoC}_2^nV_{\rm dcload}m_{\rm c}n^2\omega^2\\
&- nC_{\rm e}R_{\rm load}{\rm SoC}_1{\rm SoC}_2\omega^3\left(P_{\rm o1}V_{\rm oe2}{\rm SoC}_1^{n-1}\right.\\
&\left.+ P_{\rm o2}V_{\rm oe1}{\rm SoC}_2^{n-1}\right)\\
&- 2m_{\rm c}n\omega^3C_{\rm e}{\rm SoC}_1^n{\rm SoC}_2^nV_{\rm dcload}\left(P_{\rm o1}{\rm SoC}_2V_{\rm oe2}\right.\\
&\left.+ P_{\rm o2}{\rm SoC}_1V_{\rm oe1}\right)\\
D_{\rm c} =& 2P_{\rm o1}P_{\rm o2}{\rm SoC}_1^n{\rm SoC}_2^nV_{\rm dcload}m_{\rm c}n^2\omega^3.
\end{aligned}$$

Similar as the analysis in the charging process, in the discharging process, combining (1) and (5), and perturbing the result, it yields

$$m_{\rm d}\cdot\hat{P}_{\rm oi} = n{\rm SoC}_{\rm i}^{n-1}\left(V_{\rm dc}^*-V_{\rm dci}\right)\cdot\hat{\rm SoC}_{\rm i} - {\rm SoC}_{\rm i}^{n}\cdot\hat{v}_{\rm dci}. \quad (23)$$

Combining (16) and (23), it is reached

$$\hat{P}_{\rm oi} = \frac{\lambda_{\rm i}{\rm SoC}_{\rm i}^{n}}{m_{\rm d}\lambda_{\rm i}+n{\rm SoC}_{\rm i}^{n-1}\left(V_{\rm dc}^*-V_{\rm dci}\right)}\cdot\hat{v}_{\rm dci}. \quad (24)$$

Meanwhile, considering the power matching in the system and the expressions in (3), (20), and (24), it is derived that

$$\sum_{\rm r=1}^{k}\frac{\lambda_{\rm r}{\rm SoC}_{\rm r}^{n}}{m_{\rm d}\lambda_{\rm r}+n{\rm SoC}_{\rm r}^{n-1}\left(V_{\rm dc}^*-V_{\rm dci}\right)} = \frac{2V_{\rm dcload}G_{\rm lpf}}{R_{\rm load}}. \quad (25)$$

Hence, by taking the system with two ESUs as an example, the characteristic equation can be obtained as

$$A_{\rm d}\cdot s^3 + B_{\rm d}\cdot s^2 + C_{\rm d}\cdot s + D_{\rm d} = 0 \quad (26)$$

where

$$\begin{aligned}
A_{\rm d} =& C_{\rm e}^2R_{\rm load}{\rm SoC}_1{\rm SoC}_2V_{\rm oe1}V_{\rm oe2}m_{\rm d}\omega_{\rm c}^2\left({\rm SoC}_1^n+{\rm SoC}_2^n\right)\\
&+ C_{\rm e}R_{\rm load}{\rm SoC}_1^n{\rm SoC}_2^nn\omega_{\rm c}\left({\rm SoC}_2V_{\rm dcref}V_{\rm oe2}\right.\\
&\left.+ {\rm SoC}_1V_{\rm dcref}V_{\rm oe1}\right)\\
&- C_{\rm e}R_{\rm load}{\rm SoC}_1^n{\rm SoC}_2^nn\omega_{\rm c}\left({\rm SoC}_2V_{\rm dc1}V_{\rm oe2}\right.\\
&\left.+ {\rm SoC}_1V_{\rm dc2}V_{\rm oe1}\right)\\
B_{\rm d} =& 2{\rm SoC}_1^n{\rm SoC}_2^nV_{\rm dcload}n^2\omega_{\rm c}\left(V_{\rm dcref}-V_{\rm dc1}\right)\left(V_{\rm dcref}-V_{\rm dc2}\right)
\end{aligned}$$

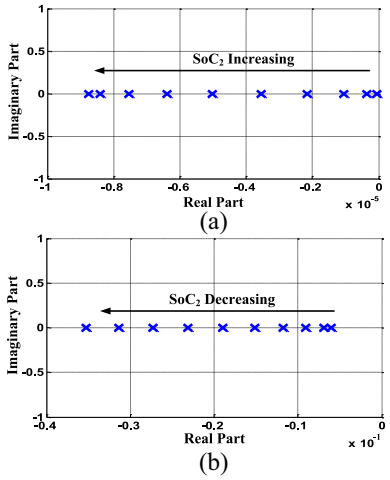

Fig. 7. Dominant poles of double-quadrant SoC-based droop control method. (a) Charging process. (b) Discharging process.

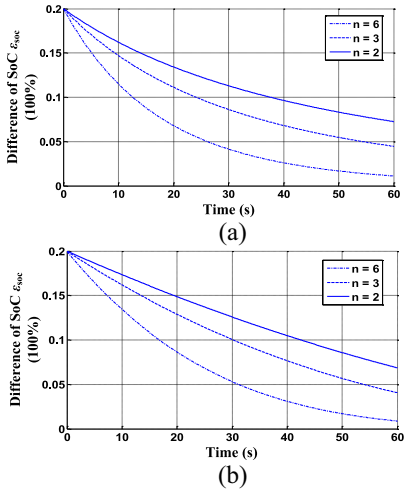

Fig. 8. Final errors of SoC with different exponent n.

$$
\begin{aligned}
&+ C_{\mathrm{e}}^2 \mathrm{SoC}_1 \mathrm{SoC}_2 V_{\mathrm{oe1}} V_{\mathrm{oe2}} m_{\mathrm{d}} \omega_{\mathrm{c}}^3 \left(2V_{\mathrm{dcload}} m_{\mathrm{d}} \right. \\
&\qquad \left. + R_{\mathrm{load}} \mathrm{SoC}_2^n\right) \\
&+ C_{\mathrm{e}}^2 \mathrm{SoC}_1 \mathrm{SoC}_2 V_{\mathrm{oe1}} V_{\mathrm{oe2}} m_{\mathrm{d}} \omega_{\mathrm{c}}^3 \cdot R_{\mathrm{load}} \mathrm{SoC}_1^n \\
&+ 2C_{\mathrm{e}} R_{\mathrm{load}} \mathrm{SoC}_1^n \mathrm{SoC}_2^n n \omega_{\mathrm{c}}^2 \left(\mathrm{SoC}_2 V_{\mathrm{dcref}} V_{\mathrm{oe2}} \right. \\
&\qquad \left. + \mathrm{SoC}_1 V_{\mathrm{dcref}} V_{\mathrm{oe1}}\right) \\
&- 2C_{\mathrm{e}} R_{\mathrm{load}} \mathrm{SoC}_1^n \mathrm{SoC}_2^n n \omega_{\mathrm{c}}^2 \left(\mathrm{SoC}_2 V_{\mathrm{dc1}} V_{\mathrm{oe2}} \right. \\
&\qquad \left. + \mathrm{SoC}_1 V_{\mathrm{dc2}} V_{\mathrm{oe1}}\right) \\
&+ 2C_{\mathrm{e}} \mathrm{SoC}_1 \mathrm{SoC}_2 V_{\mathrm{dcload}} m_{\mathrm{d}} n \omega_{\mathrm{c}}^2 \left(\mathrm{SoC}_1^{n-1} V_{\mathrm{dcref}} V_{\mathrm{oe2}} \right. \\
&\qquad \left. + \mathrm{SoC}_2^{n-1} V_{\mathrm{dcref}} V_{\mathrm{oe1}}\right) \\
&- 2C_{\mathrm{e}} \mathrm{SoC}_1 \mathrm{SoC}_2 V_{\mathrm{dcload}} m_{\mathrm{d}} n \omega_{\mathrm{c}}^2 \left(\mathrm{SoC}_1^{n-1} V_{\mathrm{dc1}} V_{\mathrm{oe2}} \right. \\
&\qquad \left. + \mathrm{SoC}_2^{n-1} V_{\mathrm{dc2}} V_{\mathrm{oe1}}\right)
\end{aligned}
$$

$$
\begin{aligned}
C_{\mathrm{d}} = {} & 4\mathrm{SoC}_1^n \mathrm{SoC}_2^n V_{\mathrm{dcload}} n^2 \omega_{\mathrm{c}}^2 \left(V_{\mathrm{dcref}} - V_{\mathrm{dc1}}\right)\left(V_{\mathrm{dcref}} - V_{\mathrm{dc2}}\right) \\
&+ C_{\mathrm{e}} R_{\mathrm{load}} \mathrm{SoC}_1^n \mathrm{SoC}_2^n n \omega_{\mathrm{c}}^3 \left(\mathrm{SoC}_2 V_{\mathrm{dcref}} V_{\mathrm{oe1}} \right. \\
&\qquad \left. + \mathrm{SoC}_1 V_{\mathrm{dcref}} V_{\mathrm{oe2}}\right) \\
&- C_{\mathrm{e}} R_{\mathrm{load}} \mathrm{SoC}_1^n \mathrm{SoC}_2^n n \omega_{\mathrm{c}}^3 \left(\mathrm{SoC}_2 V_{\mathrm{dc1}} V_{\mathrm{oe2}} \right. \\
&\qquad \left. + \mathrm{SoC}_1 V_{\mathrm{dc2}} V_{\mathrm{oe1}}\right) \\
&+ 2C_{\mathrm{e}} \mathrm{SoC}_1 \mathrm{SoC}_2 V_{\mathrm{dcload}} m_{\mathrm{d}} n \omega_{\mathrm{c}}^3 \left(\mathrm{SoC}_1^{n-1} V_{\mathrm{dcref}} V_{\mathrm{oe2}} \right. \\
&\qquad \left. + \mathrm{SoC}_2^{n-1} V_{\mathrm{dcref}} V_{\mathrm{oe1}}\right) \\
&- 2C_{\mathrm{e}} \mathrm{SoC}_1 \mathrm{SoC}_2 V_{\mathrm{dcload}} m_{\mathrm{d}} n \omega_{\mathrm{c}}^3 \left(\mathrm{SoC}_1^{n-1} V_{\mathrm{dc1}} V_{\mathrm{oe2}} \right. \\
&\qquad \left. + \mathrm{SoC}_2^{n-1} V_{\mathrm{dc2}} V_{\mathrm{oe1}}\right) \\
D_{\mathrm{d}} = {} & 2\mathrm{SoC}_1^n \mathrm{SoC}_2^n V_{\mathrm{dcload}} n^2 \omega_{\mathrm{c}}^3 \left(V_{\mathrm{dcref}} - V_{\mathrm{dc1}}\right)\left(V_{\mathrm{dcref}} - V_{\mathrm{dc2}}\right).
\end{aligned}
$$

By using the characteristic equations for the charging and discharging operation modes, the dominant poles of the system can be reached, as shown in Fig. 7. Since the ESU is equivalent to each other in the system, it is set that SoC_1 is kept constant while SoC_2 varies in the feasible range. It is found that all the dominant poles of the system locate in the left half of s domain, which indicates that the system stability is guaranteed in both charging and discharging processes.

C. Speed Regulation of SoC Balancing

As mentioned in Section I, the exponent n is employed in the proposed double-quadrant SoC-based droop control method to reach the speed regulation of SoC balancing and injected/output power equalization. Here, the variables $\varepsilon_{\mathrm{socT}}$ and $\varepsilon_{\mathrm{poT}}$ are involved, which define the errors of SoC and injected/output power after time period T. The variables satisfy the following expressions:

$$\varepsilon_{\mathrm{socT}} = \left| \max_{\mathrm{i}=1,2,\ldots,\mathrm{k}} \{\mathrm{SoC}_{\mathrm{i\,t=T}}\} - \min_{\mathrm{i}=1,2,\ldots,\mathrm{k}} \{\mathrm{SoC}_{\mathrm{i\,t=T}}\} \right| \quad (27)$$

$$\varepsilon_{\mathrm{poT}} = \left| \max_{\mathrm{i}=1,2,\ldots,\mathrm{k}} \{p_{\mathrm{oi\,t=T}}\} - \min_{\mathrm{i}=1,2,\ldots,\mathrm{k}} \{p_{\mathrm{oi\,t=T}}\} \right| \quad (28)$$

where $\mathrm{SoC}_{\mathrm{it=T}}$ and $p_{\mathrm{oi\,t=T}}$ are the SoC and injected/output power when $t = T$.

By using the same parameters as in Table I, the errors of SoC ($\varepsilon_{\mathrm{socT}}$) with different exponent n are shown in Fig. 8(a) and (b). Here, the labeled subparts in Fig. 8 shows the different values of exponent n, which is selected in the control diagram. It is found that in both charging and discharging process, the larger exponent n is selected, the smaller final error of SoC can be reached, meaning that the speed of SoC balancing increases.

D. Saturation Limiter Used for Starting Process

During the starting process, with larger exponent n, the difference of initial SoC^n becomes larger, which results in larger difference in the initial injected/output power. In order to avoid that the injected/output power exceeds the maximum acceptable power, a saturation limiter is employed. In particular, when the estimated injected/output power exceeds the upper limit, it is limited to the maximum power. The above objective can be reached by involving a power-controlled operation mode. In the starting process, the system initially operates in the voltage-controlled operation mode and the double-quadrant SoC-based droop control method is used. If the estimated injected/output power exceeds the upper limits, the operation mode of the corresponding interfacing converter is switched from voltage-controlled mode to power-controlled mode.

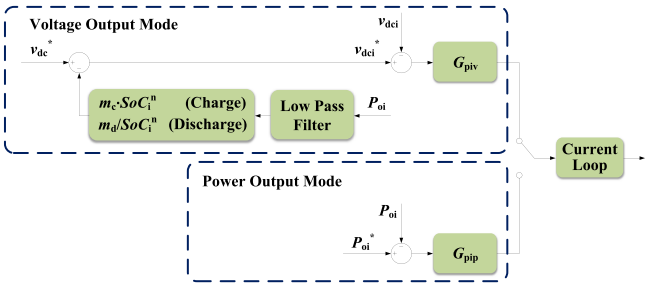

Fig. 9. Control diagram for the voltage and power controlled operation modes.

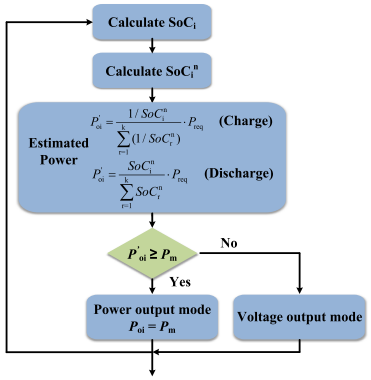

Fig. 10. Flow chart for the selection of different operation mode in the starting process.

Meanwhile, the power reference value of the power-controlled operation mode is set to be the maximum acceptable value. When the estimated injected/output power becomes lower than the upper limits, the operation mode of the related converter is switched back from power-controlled mode to voltage-controlled mode. The difference between the voltage and power controlled operation modes is essentially different methods of generating the reference values for the inner current loop, as shown in Fig. 9. The flow chart for the selection of different operation modes in the starting process is shown in Fig. 10.

E. Limitations of Parameters Used in Control Diagram

The limitations of the parameters used in the double-quadrant SoC-based droop control method are studied in this subsection. In general, two constraints should be considered. They are SoC balancing speed and dc voltage deviation, respectively. For the first constraint, the SoC balancing should reach the desired speed. This is achieved by adjusting the value of exponent n. In particular, for the existing system parameters, by combining (10) and (11), or (10) and (12), the numeric solutions of SoC can be derived in the charging or discharging process, as shown in Fig. 6. Hence, $\varepsilon_{\mathrm{SoCT}}$ can be obtained within a preset time period T. The variable $\varepsilon_{\mathrm{SoCT}}$ should be lower than its maximum value by tuning the exponent n. Therefore, the required exponent n can be reached to guarantee the desired SoC balancing speed. In the given system, the exponent n is selected as 6. It should be noticed that the exponent n here is its minimum value. Theoretically, it can be larger to get a higher convergence speed. However, in a practical application, over-rapid charging or discharging may have negative impact on ESU. As a result, only the minimum value of exponent n is selected.

For the second constraint, in order to ensure the normal operation of the system, the dc voltage deviation should be neither too large nor too small. If the dc voltage deviation is too large, the stability of the system cannot be guaranteed. Meanwhile, since droop control works with the dc voltage deviation, if it is too small, the performance of droop control is influenced. Hence, the following inequalities should be satisfied. Here, the exponent n derived in the first step is used to keep the required SoC balancing speed.

In the charging process

$$\begin{cases} m_{\mathrm{c}} \mathrm{SoC}_{\max}^{n} \cdot P_{\mathrm{omax}} \leq \Delta v_{\mathrm{dcmax}} \\ m_{\mathrm{c}} \mathrm{SoC}_{\min}^{n} \cdot P_{\mathrm{omin}} \geq \Delta v_{\mathrm{dcmin}} \end{cases} \tag{29}$$

where $\mathrm{SoC}_{\max}$ and $\mathrm{SoC}_{\min}$ are the maximum and minimum values of SoC, P_{omax}, and P_{omin} are the maximum and minimum values of injected/output power, $\Delta v_{\mathrm{dcmax}}$ and $\Delta v_{\mathrm{dcmin}}$ are the maximum and minimum values of dc voltage deviation.

In the discharging process

$$\begin{cases} \dfrac{m_{\mathrm{d}}}{\mathrm{SoC}_{\min}^{n}} \cdot P_{\mathrm{omax}} \leq \Delta v_{\mathrm{dcmax}} \\ \dfrac{m_{\mathrm{d}}}{\mathrm{SoC}_{\max}^{n}} \cdot P_{\mathrm{omin}} \geq \Delta v_{\mathrm{dcmin}} \end{cases}. \tag{30}$$

For example, assuming that $35\% \leq \mathrm{SoC} \leq 95\%$ and $0.2\ \mathrm{kW} \leq P_{\mathrm{o}} \leq 2.5\ \mathrm{kW}$, (29) and (30) can be solved. It is calculated that the feasible range of the initial droop coefficients in charging and discharging process is shown as $5.4 \times 10^{-3} \leq m_{\mathrm{c}} \leq 6.5 \times 10^{-3}$, $7.4 \times 10^{-6} \leq m_{\mathrm{d}} \leq 8.8 \times 10^{-6}$, with the exponent $n = 6$.

Meanwhile, in Section III-D, the saturation unit is employed to limit the injected/output power during starting process. It can be regarded as a protective unit to avoid that the injected/output power exceeds the maximum acceptable value. In order to further reveal the relationship between the selection of exponent n and the initial power distribution, Fig. 11 is shown here. During the starting period, as shown in Fig. 11(a), in the charging process, the difference of the initial injected power becomes larger when the exponent n increases. At the same time, in the discharging process, the difference of the initial output power also becomes larger when the exponent n increases, as shown in Fig. 11(b).

It should be noted that in practical applications the charging and discharging speed for ESU is related to different factors, i.e., service life, reliability, overall system efficiency, etc. Since the control diagram design for DESUs is the main research focus in this paper, the ESU itself has not been discussed in detail. From the view of applying the proposed method in practical applications, the selection of the key parameters can be slightly tuned around the theoretical values.

IV. Simulation Validation

Simulation model comprised of three ESUs is implemented by using MATLAB/simulink to validate the proposed double-quadrant SoC-based droop control method. Different cases are studied to test the feasibility of the proposed method.

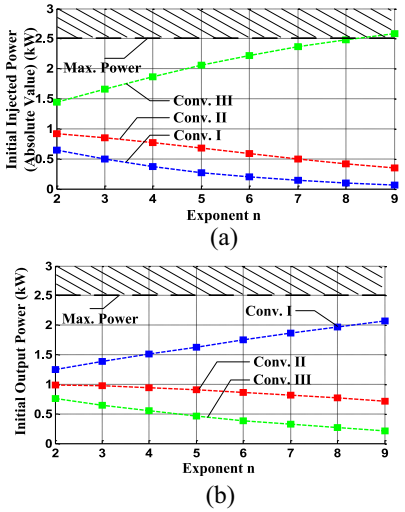

Fig. 11. Initial injected/output power with different exponent n. (a) Charging process. (b) Discharging process.

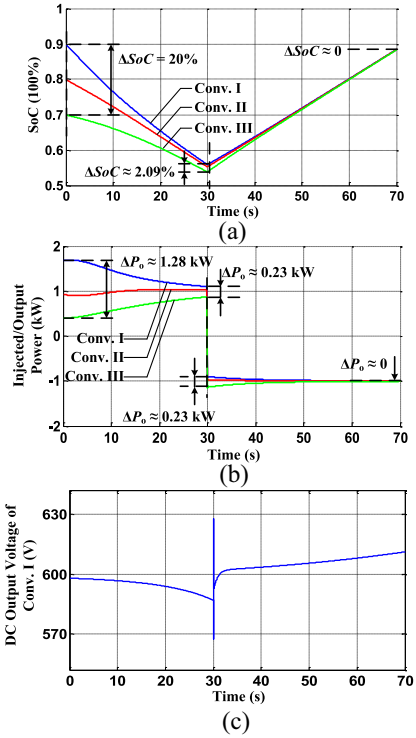

Fig. 12. Mode transferring from discharging to charging (SoC balanced after the mode transferring). (a) Waveforms of SoC. (b) Waveforms of injected/output power. (c) Waveform of dc output voltage for converter I.

A. Case I. Transferring Between Charging and Discharging Operation Modes

The transferring between charging and discharging process is tested. In Fig. 12, the ESUs first operate in discharging mode, and then change to charging mode. During the discharging operation, $\varepsilon_{\mathrm{SoC}}$ is reduced from 20% to 2.09% with the proposed SoC-based droop control method, and the $\varepsilon_{\mathrm{po}}$ is reduced from 1.28 to 0.23 kW. Then, in the charging period, the SoC is gradually balanced and the injected power is equalized. The dc output voltage waveform of converter I during the discharging and charging process is shown in Fig. 12(c). It is seen that the dc voltage is limited within the acceptable range.

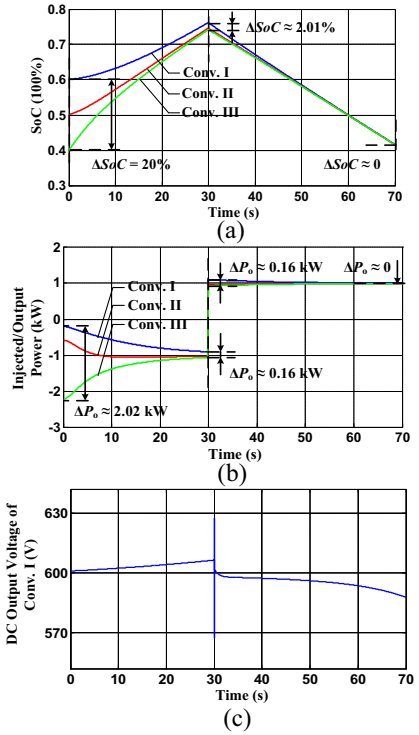

Fig. 13. Mode transferring from charging to discharging (SoC balanced after the mode transferring). (a) Waveforms of SoC. (b) Waveforms of injected/output power. (c) Waveform of dc output voltage for converter I.

In Fig. 13, the ESUs first operate in charging mode, and then change to discharging mode. With the proposed SoC-based droop control method, $\varepsilon_{\mathrm{SoC}}$ is reduced from 20% to 2.01% during the charging process, and the $\varepsilon_{\mathrm{po}}$ is reduced from 2.02 to 0.16 kW. In the following discharging process, the balanced SoC and equalized output power are gradually achieved. The dc output voltage waveform of converter I during the charging and discharging process is shown in Fig. 13(c). It is seen that the dc voltage is also limited within the acceptable range.

B. Case II. Dynamic Responses With ESU Disconnection

The dynamic response with ESU disconnection is shown below. As shown in Fig. 14, all of the three ESUs operate in the charging mode. Since the SoC-based droop control method is used, the SoCs are gradually balanced and the injected power is equalized. In the period of 0–15 s, it is seen that $\varepsilon_{\mathrm{SoC}}$ changes from 20% to 6.23% and $\varepsilon_{\mathrm{SoC}}$ changes from 1.76 to 0.82 kW. At t = 15 s, ESU #1 is disconnected. ESU #2 and #3 continue absorbing power. The SoC and injected power still gradually become equal respectively. It is also seen that in the period of 15–30 s, $\varepsilon_{\mathrm{SoC}}$ changes from 0.98% to almost zero and $\varepsilon_{\mathrm{po}}$ changes from 0.11 kW to almost zero. At t = 30 s, ESU #2 is disconnected. Only ESU #3 remains working and continues absorbing power. It can be found that in the

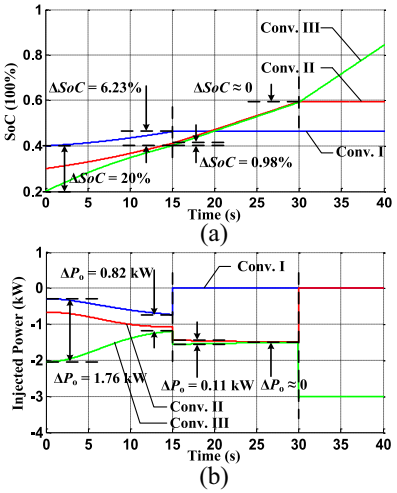

Fig. 14. Charging process with dynamic disconnection of ESUs. (a) Waveforms of SoC. (b) Waveforms of injected power.

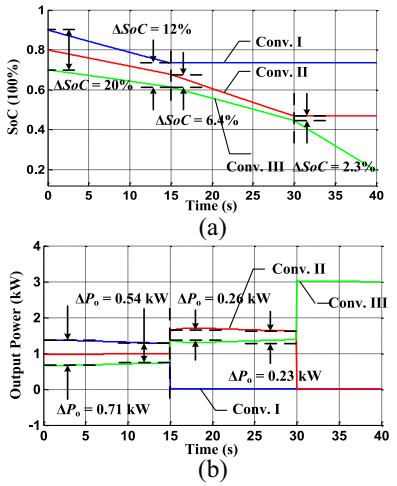

Fig. 15. Discharging process with dynamic disconnection of ESUs. (a) Waveforms of SoC. (b) Waveforms of output power.

whole process with dynamic disconnection, the system keeps stable. The SoC-based droop control method works properly.

In the discharging process, three ESUs are used together to deliver power, as shown in Fig. 15. In the period of 0–15 s, $\varepsilon_{\mathrm{SoC}}$ changes from 20% to 12% and $\varepsilon_{\mathrm{po}}$ changes from 0.71 to 0.54 kW. At t = 15 s, ESU #1 is disconnected, ESU #2 and #3 continue delivering power. In the period of 15–30 s, $\varepsilon_{\mathrm{SoC}}$ changes from 6.4% to 2.3% and $\varepsilon_{\mathrm{po}}$ changes from 0.26 to 0.23 kW. At t = 30 s, ESU #2 is disconnected. Only ESU #3 remains in the system. It is found that during the whole discharging process with dynamic disconnecting of ESUs, the SoC-based control system keeps stable.

C. Case III. Speed Regulation With Different Exponent n

In order to show the speed regulation with different exponent n, the final errors of SoC for both charging and discharging process after the same time period are shown in Fig. 16. It is concluded that with higher exponent n, the final error

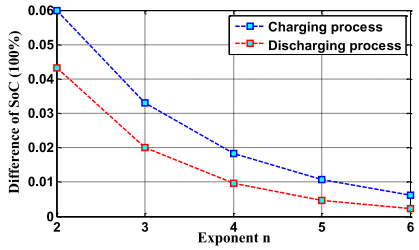

Fig. 16. Final errors of SoC with different exponent n.

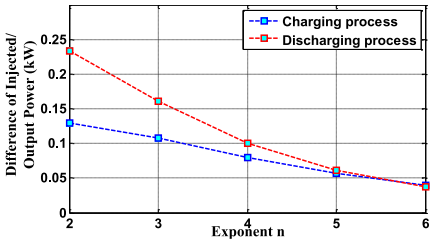

Fig. 17. Final errors of injected/output power with different exponent n.

of SoC becomes smaller. When the exponent n changes from 2 to 6, the final error of SoC reduces from 6% to 0.7% in the charging process and it reduces from 4.3% to 0.2% in the discharging process. Meanwhile, similar results can be found in the final errors of injected/output power, as shown in Fig. 17. When the exponent n changes from 2 to 6, the final error of injected power reduces from 0.24 to 0.04 kW in the charging process and it reduces from 0.13 to 0.04 kW in the discharging process. With larger exponent, the power equalization speed is enhanced.

D. Case IV. Saturation Limits During Starting Process

The saturation limiter is employed to avoid that the injected/output power exceeds the maximum acceptable value. In order to see its effectiveness, the absolute value of the required power from the ESUs is increased to 5 kW. The waveforms of SoC and injected/output power in both charging and discharging process are shown in Figs. 18 and 19.

It is seen that in the charging process, for ESU #3, the injected power gets to its maximum limits. Hence, the control diagram of this converter changes from voltage-controlled mode to power-controlled mode. The injected power remains at its maximum value, which is 2.5 kW. Meanwhile, the other two ESUs operate at voltage-controlled mode with double-quadrant SoC-based droop control method. The error of SoC_1 and SoC_2 is reduced from 10% to 3.11%, and the error of injected power is reduced from 0.59 to 0.23 kW. At t = 40 s, the estimated injected power of ESU #3 becomes lower than the maximum value, so it changes back to voltage-controlled operation mode, and the required power is shared by all of the three converters. In the following 20 s, $\varepsilon_{\mathrm{SoC}}$ (calculated among three ESUs) is reduced from 4.44% to 1.16%, and the injected power is reduced from 0.87 to 0.19 kW.

In the discharging process, the output power of ESU #1 reaches its maximum value. Hence, it changes to power-controlled operation mode and the output power reference is set to the maximum acceptable value 2.5 kW. At the

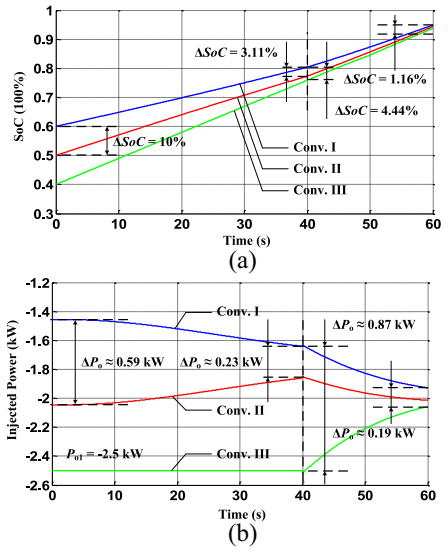

Fig. 18. Effect of saturation limiter in the charging process. (a) Waveforms of SoC. (b) Waveforms of injected power.

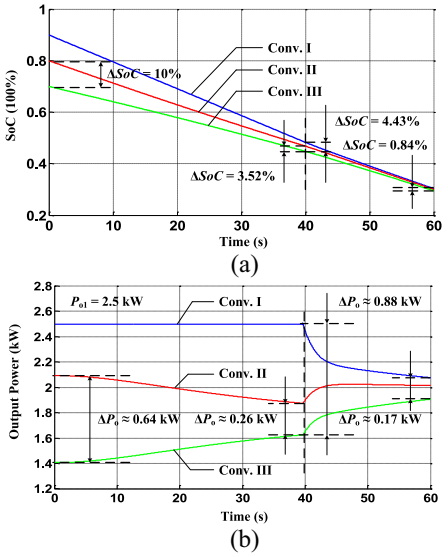

Fig. 19. Effect of saturation limiter in the discharging process. (a) Waveforms of SoC. (b) Waveforms of output power.

same time, the other two ESUs operate at voltage-controlled mode with double-quadrant SoC-based droop control method. The error of SoC_1 and SoC_2 is reduced from 10% to 3.52%, and the error of output power is reduced from 0.64 to 0.26 kW. At t = 40 s, the estimated output power of ESU #1 becomes lower than the maximum value, so it changes back to voltage-controlled operation mode, and the required power is shared by all of the three converters. In the following 20 s, ε_{SoC} (calculated among three ESUs) is reduced from 4.43% to 0.84%, and the output power is reduced from 0.88 to 0.17 kW.

V. Conclusion

In this paper, the SoC-based droop control method is proposed to reach the proper power sharing between different ESUs in autonomous dc microgrids. Both charging and discharging operation modes are taken into account. In the charging process, the droop coefficient is set to be proportional to the SoC^n, while in the discharging process, the droop coefficient is set to be inversely proportional to the SoC^n. It is demonstrated that with the proposed double-quadrant SoC-based droop control method, SoC balancing and injected/output power equalization can be achieved in both charging and discharging modes. The exponent n is employed to adjust the balancing speed. It is found that with higher exponent n, the balancing speed is enhanced. Limits of the parameters in the control scheme are discussed by considering the boundaries employed by SoC balancing speed and dc voltage deviation. By selecting the reasonable parameters, the stability of the control system is ensured.

References

[1] Y. J. Reddy, Y. V. P. Kumar, K. P. Raju, and A. Ramsesh, "Retrofitted hybrid power system design with renewable energy sources for buildings," *IEEE Trans. Smart Grid*, vol. 3, no. 4, pp. 2174–2187, Dec. 2012.

[2] Q. Fu *et al.*, "Transition management of microgrids with high penetration of renewable energy," *IEEE Trans. Smart Grid*, vol. 5, no. 2, pp. 539–549, Mar. 2014.

[3] F. Katiraei and M. R. Iravani, "Power management strategies for a microgrid with multiple distributed generation units," *IEEE Trans. Power Syst.*, vol. 21, no. 4, pp. 1821–1831, Nov. 2006.

[4] Y. W. Li and C. N. Kao, "An accurate power control strategy for power-electronics-interfaced distributed generation units operating in a low-voltage multibus microgrid," *IEEE Trans. Power Electron.*, vol. 24, no. 12, pp. 2977–2988, Dec. 2009.

[5] Q. C. Zhong, "Robust droop controller for accurate proportional load sharing among inverters operated in parallel," *IEEE Trans. Ind. Electron.*, vol. 60, no. 4, pp. 1281–1290, Apr. 2013.

[6] C. K. Sao and P. W. Lehn, "Autonomous load sharing of voltage source converters," *IEEE Trans. Power Del.*, vol. 20, no. 2, pp. 1009–1016, Apr. 2005.

[7] J. C. Vasquez, J. M. Guerrero, M. Savaghebi, J. Eloy-Garcia, and R. Teodorescu, "Modeling, analysis, and design of stationary-reference-frame droop-controlled parallel three-phase voltage source inverters," *IEEE Trans. Ind. Electron.*, vol. 60, no. 4, pp. 1271–1280, Apr. 2013.

[8] N. Pogaku, M. Prodanoviæ, and T. C. Green, "Modeling, analysis and testing of autonomous operation of an inverter-based microgrid," *IEEE Trans. Power Electron.*, vol. 22, no. 2, pp. 613–625, Mar. 2007.

[9] A. Pratt, P. Kumar, and T. V. Aldridge, "Evaluation of 400V DC distribution in telco and data centers to improve energy efficiency," in *Proc. Int. Telecommun. Energy Conf. (INTELEC)*, Rome, Italy, 2007, pp. 32–39.

[10] S. R. Huddy and J. D. Skufca, "Amplitude death solutions for stabilization of DC microgrids with instantaneous constant-power loads," *IEEE Trans. Power Electron.*, vol. 28, no. 1, pp. 247–253, Jan. 2013.

[11] H. Kakigano, Y. Miura, and T. Ise, "Distribution voltage control for DC microgrids using fuzzy control and gain-scheduling technique," *IEEE Trans. Power Electron.*, vol. 28, no. 5, pp. 2246–2258, May 2013.

[12] K. Sun, L. Zhang, Y. Xing, and J. M. Guerrero, "A distributed control strategy based on DC bus signaling for modular photovoltaic generation systems with battery energy storage," *IEEE Trans. Power Electron.*, vol. 26, no. 10, pp. 3032–3045, Oct. 2011.

[13] D. Dong *et al.*, "Grid-interface bi-directional converter for residential DC distribution systems—-Part one: High-density two-stage topology," *IEEE Trans. Power Electron.*, vol. 28, no. 4, pp. 1655–1666, Apr. 2013.

[14] X. Lu, K. Sun, J. M. Guerrero, and L. Huang, "State-of-charge balance using adaptive droop control for distributed energy storage systems in DC micro-grid applications," *IEEE Trans. Ind. Electron.*, vol. 61, no. 6, pp. 2804–2815, Jan. 2014.

[15] X. Lu, J. M. Guerrero, K. Sun, and J. C. Vasquez, "An improved control method for DC microgrids based on low bandwidth communication with DC bus voltage restoration and enhanced current sharing accuracy," *IEEE Trans. Power Electron.*, vol. 29, no. 4, pp. 1800–1812, Apr. 2014.

[16] X. Lu *et al.*, "Hierarchical control of parallel AC–DC converter interfaces for hybrid microgrids," *IEEE Trans. Smart Grid*, vol. 5, no. 2, pp. 683–692, Mar. 2014.

[17] J. M. Carrasco *et al.*, "Power-electronic systems for the grid integration of renewable energy sources: A survey," *IEEE Trans. Ind. Electron.*, vol. 53, no. 4, pp. 1002–1016, Jun. 2006.
[18] J. Rajagopalan, K. Xing, Y. Guo, and F. C. Lee, "Modeling and dynamic analysis of paralleled DC/DC converters with master-slave current sharing control," in *Proc. Appl. Power Electron. Conf. Expo. (APEC)*, San Jose, CA, USA, 1996, pp. 678–684.
[19] T. F. Wu, Y. K. Chen, and Y. H. Huang, "3C strategy for inverters in parallel operation achieving an equal current distribution," *IEEE Trans. Ind. Electron.*, vol. 47, no. 2, pp. 273–281, Apr. 2000.
[20] X. Sun, Y. S. Lee, and D. H. Xu, "Modeling, analysis, and implementation of parallel multi-inverter systems with instantaneous average-current-sharing scheme," *IEEE Trans. Power Electron.*, vol. 18, no. 3, pp. 844–856, May 2003.
[21] E. Alegria, T. Brown, E. Minear, and R. H. Lasseter, "CERTS microgrid demonstration with large-scale energy storage and renewable generation," *IEEE Trans. Smart Grid*, vol. 5, no. 2, pp. 937–943, Mar. 2014.
[22] H.-S. Park, C.-E. Kim, C.-H. Kim, G.-W. Moon, and J.-H. Lee, "A modularized charge equalizer for an HEV lithium-ion battery string," *IEEE Trans. Ind. Electron.*, vol. 56, no. 5, pp. 1464–1476, May 2009.
[23] A. Manenti, A. Abba, A. Merati, S. M. Savaresi, and A. Geraci, "A new BMS architecture based on cell redundancy," *IEEE Trans. Ind. Electron.*, vol. 58, no. 9, pp. 4314–4322, Sep. 2011.
[24] J. Kim, J. Shin, C. Chun, and B. H. Cho, "Stable configuration of a Li-ion series battery pack based on a screening process for improved voltage/SoC balancing," *IEEE Trans. Power Electron.*, vol. 27, no. 1, pp. 411–424, Jan. 2012.
[25] L. Maharjan, S. Inoue, H. Akagi, and J. Asakura, "State-of-charge (SoC)—Balancing control of a battery energy storage system based on a cascade PWM converter," *IEEE Trans. Power Electron.*, vol. 24, no. 6, pp. 1628–1636, Jun. 2009.
[26] P. Cairoli, I. Kondratiev, and R. A. Dougal, "Coordinated control of the bus tie switches and power supply converters for fault protection in DC microgrids," *IEEE Trans. Power Electron.*, vol. 28, no. 4, pp. 2037–2047, Apr. 2013.
[27] *XLPE Insulated Cables of Rated Voltages up to 0,6/1 kV With Crosslinked Polymer*, Standards BT 2006/95/EC - RoHS: 2002/95/EC, General Cavi Catalog.

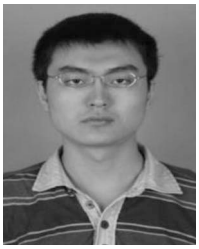

Xiaonan Lu (S'11–M'14) was born in Tianjin, China, in 1985. He received the B.E. and Ph.D. degrees in electrical engineering from Tsinghua University, Beijing, China, in 2008 and 2013, respectively.

From 2010 to 2011, he was a Guest Ph.D. Student with the Department of Energy Technology, Aalborg University, Aalborg, Denmark. He joined the Department of Electrical Engineering and Computer Science, University of Tennessee, Knoxville, TN, USA, in 2013, where he is currently a Post-Doctoral Research Associate. His current research interests include control of power electronics interfacing converters for renewable generation systems and microgrids, hardware-in-the-loop real-time test, multilevel converters, and matrix converters.

Dr. Lu was the recipient of the Outstanding Reviewer Award for the IEEE TRANSACTION ON POWER ELECTRONICS in 2014. He is a member of Industrial Electronics Society and Power Electronics Society.

Kai Sun (M'12) was born in Beijing, China, in 1977. He received the B.E., M.E., and Ph.D. degrees in electrical engineering from Tsinghua University, Beijing, China, in 2000, 2002, and 2006, respectively.

He joined the Faculty of Tsinghua University as a Lecturer with the Department of Electrical Engineering, in 2006, where he is currently an Associate Professor. From 2009 to 2010, he was a Visiting Scholar with the Department of Energy Technology, Aalborg University, Aalborg, Denmark. His current research interests include power converters for renewable generation systems and microgrids. He has authored over 100 technical papers, including 21 international journal papers.

Dr. Sun was the recipient of the Delta Young Scholar Award in 2013.

Josep M. Guerrero (S'01–M'04–SM'08) received the B.S. degree in telecommunications engineering, the M.S. degree in electronics engineering, and the Ph.D. degree in power electronics from the Technical University of Catalonia, Barcelona, Spain, in 1997, 2000, and 2003, respectively.

He was an Associate Professor with the Department of Automatic Control Systems and Computer Engineering, Technical University of Catalonia, where he was involved in teaching courses on digital signal processing, field-programmable gate arrays, microprocessors, and control of renewable energy. In 2004, he was responsible for the Renewable Energy Laboratory, Escola Industrial de Barcelona, Barcelona. Since 2011, he has been a Full Professor with the Department of Energy Technology, Aalborg University, Aalborg, Denmark, where he was responsible for the microgrid research program. Since 2012, he has been a Guest Professor with the Chinese Academy of Science, Beijing, China, and the Nanjing University of Aeronautics and Astronautics, Nanjing, China, and also a Guest Professor with the Control Science and Engineering College, Shandong University, Jinan, China, since 2013. His current research interests include different microgrid aspects, including power electronics, distributed energy-storage systems, hierarchical and cooperative control, energy management systems, and optimization of microgrids and islanded minigrids.

Prof. Guerrero was the recipient of the Institute for Scientific Information Highly Cited Researcher by T. Reuters in 2014. He is an Associate Editor for the IEEE TRANSACTIONS ON POWER ELECTRONICS, the IEEE TRANSACTIONS ON INDUSTRIAL ELECTRONICS, and the IEEE INDUSTRIAL ELECTRONICS MAGAZINE, and an Editor for the IEEE TRANSACTIONS ON SMART GRID. He has been a Guest Editor for the IEEE TRANSACTIONS ON POWER ELECTRONICS special issues: Power Electronics for Wind Energy Conversion and Power Electronics for Microgrids, the IEEE TRANSACTIONS ON INDUSTRIAL ELECTRONICS special sections: Uninterruptible Power Supplies Systems, Renewable Energy Systems, Distributed Generation, and Microgrids, and Industrial Applications and Implementation Issues of the Kalman Filter, and the IEEE TRANSACTIONS ON SMART GRID special issue: Smart DC Distribution Systems. He was the Chair of the Renewable Energy Systems Technical Committee of the IEEE Industrial Electronics Society.

Juan C. Vasquez (M'12) received the B.S. degree in electronics engineering from the Autonoma University of Manizales, Manizales, Colombia, in 2004, and the Ph.D. degree in automatic control systems and computer engineering from the Technical University of Catalonia, Barcelona, Spain, in 2009.

He was a Post-Doctoral Assistant, responsible for teaching courses based on renewable energy systems, with the Department of Automatic Control Systems and Computer Engineering, Technical University of Catalonia. He is currently an Assistant Professor with Aalborg University, Aalborg, Denmark. His current research interests include modeling, simulation, networked control systems, and optimization for power management systems applied to distributed generation in ac/dc microgrids.

Lipei Huang was born in Jiangsu, China, in 1946. He received the B.E. and M.E. degrees in electrical engineering from Tsinghua University, Beijing, China, in 1970 and 1982, respectively, and the Ph.D. degree in electrical engineering from Meiji University, Tokyo, Japan, in 1996.

He joined the Department of Electrical Engineering, Tsinghua University, in 1970, where he has been a Professor since 1994. In 1987, he was a Visiting Scholar with the Department of Electrical Engineering, Tokyo Institute of Technology, Meguro, Japan, for three months, and with Meiji University, Kawasaki, Japan, for nine months. He joined the research projects of the K. Matsuse Laboratory, Department of Electrical Engineering, Meiji University, as a Visiting Professor in 1993. His current research interests include power electronics and adjustable-speed drives. He has authored over 100 technical papers and holds seven patents.

Prof. Huang was the recipient of education awards from the China Education Commission and Beijing People's Government in 1997. From 2001 to 2003, he was a Delta Scholar.